Numerical comparison of exhaled particle dispersion under different air distributions for winter heating

Numerical comparison of exhaled particle dispersion under different air distributions for winter heating

Teng Li[1,2], Emmanuel A. Essah[3], Yuxin Wu[4], Yong Cheng[1,2*], and Chunhui Liao[5]

[1]Joint International Research Laboratory of Green Buildings and Built Environments, Ministry of Education, Chongqing University, Chongqing, China

[2]National Centre for International Research of Low-carbon and Green Buildings, Ministry of Science & Technology, Chongqing University, Chongqing, China

[3]School of Construction Management and Engineering, The University of Reading, United Kingdom

[4]School of Civil Engineering and Architecture, Zhejiang Sci-Tech University, Zhejiang, China

[5]Institue for Health and Environment, Chongqing University of Science and Technology, Chongqing, China

*Corresponding author. Tel.: +86 2365123213; E-mail: yongcheng6@cqu.edu.cn

ABSTRACT

People pay close attention to prevent and control the airborne transmission of respiratory diseases, and effective ventilation can reduce the cross-infection risk. Nevertheless, in winter, poor indoor ventilation is common, and the survival rate of the virus is also high. The issue of cross infection in enclosed spaces should be worthy of more attention especially during winter. This study was to comprehensively compare the dispersion of exhaled particles with different diameters under different air distributions for heating. Computational fluid dynamics (CFD) method validated by experiments was utilized to model the exhaled particle dispersion in a two-person typical office under five air

distributions (i.e., Mixing Ventilation (MV), Stratum Ventilation (SV), Deflection Ventilation (DeV), Impinging Jet Ventilation (IJV), and Wall Attachment Jet ventilation (WAJ)) having potentials for heating. Results showed that different air distributions had significant impacts on the characteristics of exhaled particle dispersion in heating mode. The difference of average normalized particle concentration at the breathing zone can be up to 8 times. Additionally, the particle dispersion in winter can be distinct from that in summer due to effect of positive thermal buoyancy, especially for fine particles ($d \leq 10$ μm). With the specified conditions of this study, according to the proportions of removed exhaled particles, DeV performed best with a removal efficiency of more than 60% for fine particles, followed by SV, WAJ, and IJV. The removal efficiency for fine particles of DeV, SV, WAJ, and IJV were 61.86%, 52.43%, 38.95%, and 36.40% respectively. MV with a typical layout of high-side supply and ceiling exhaust exhibited the worst performance, with a removal efficiency of only 27.61%.

Keywords: air distributions; winter heating; CFD; exhaled particle; dispersion

Nomenclature	
a_i	Constant
Ar	Archimedes number
C_D	Drag coefficient
d	Aerodynamic diameter of exhaled particles, μm
ε	Turbulent dissipation
Φ	Normal distribution random number
F_{ai}	Additional force exerted on particles, m/s^2
F_i	external forces exerted on the particle in the i direction, m/s^2
g	Gravitational acceleration constant, m/s^2
K	Heat transfer coefficient, $W/(m^2 \cdot K)$
k	Turbulent kinetic energy
μ	Molecular viscosity of air, kg/(m·s)
Re	Reynolds number
ρ	Air density, kg/m^3
ρ_p	Particle density, kg/m^3
$\Gamma_\emptyset$	Effective diffusion coefficient
u_i	Air velocity in the i direction, m/s
$u_a^{'}$	Fluctuating component of air velocity

u_{pi}	Particle velocity in the i direction, m/s
y^+	Dimensionless distance to the solid wall
$S_\emptyset$	Source term

Abbreviations

ACH	Air Changes per Hour
CFD	Computational Fluid Dynamic
DPM	Discrete Phase Model
DV	Displacement Ventilation
DeV	Deflection Ventilation
IJV	Impinging Jet Ventilation
MAE	Mean Absolute Error
MV	Mixing Ventilation
RANS	Reynolds Averaged Navier Stokes
RMSE	Root Mean Square Error
SIMPLE	Semi-Implicit Pressure Linked Equation
SV	Stratum Ventilation
WAJ	Wall Attached Jet ventilation
WHO	World Health Organization

1. Introduction

1.1 Background of the research

Respiratory diseases caused by coronavirus have repeatedly threatened human health during the last two decades and seriously affected people's life and production [1-3]. In addition, there are some other epidemic diseases such as influenza, tuberculosis, measles, etc. These can be transmitted via three routes, namely intimate contact, airborne transmission, and fomite touching [4-5]. Human beings should intervene in the transmission of such diseases and find some effective ways to curb and reduce the losses.

Generally, there are three types of interventions for disease transmission: administrative management, engineering control, and personal protection. Engineering control is noted to have less constraints on people, and thus it is widely used. Enclosed spaces are one of the main locations for personnel infection [6-8]. This is evident in the fact that, there is a correlation between the infection case and building ventilation as demonstrated by previous studies [9-12], and most of the aggregated outbreak events have the issue of poor ventilation [7, 13]. Indoor ventilation can not only ensure that the thermal environment meets the requirements, but also improve indoor air quality [14]. Ventilation with warm air supply is considered as a potential heating method in winter [15]. The airflow generated by ventilation system is noted to affect the movement of viral particles released by infected people through respiratory activities (such as breathing, talking, singing, coughing, etc.). Zhao et al. [16] found that the concentration profile of particle and the particle fate changed greatly with different air distributions. Therefore, an appropriate and adequate air distribution method is key to reduce the airborne transmission of respiratory diseases.

To improve thermal comfort, inhaled air quality, and/or energy efficiency, some researchers proposed novel air distributions. Lin et al. [17] proposed Stratum Ventilation (SV), which located inlets at the side wall slightly above the head level of occupants to deliver fresh air directly into the

occupied zone. The results indicated that SV reduced the risk of cross infection among students in a classroom [18]. Tian et al. [19] compared the particle dispersion characteristics under SV and Displacement Ventilation (DV) in cooling mode. It was found that the risk of particle inhalation under SV was lower than that under DV, which was attributed to the prominently higher particle deposition fraction under SV. In hospital wards, Lu et al. [20, 21] found that SV can quickly dilute the particles compared with traditional Mixing Ventilation (MV) and DV. Kong et al. [22] experimentally investigated the control effect of different ventilation systems on fine particles, which showed that SV can minimize the airborne virus contamination. In addition, Impinging Jet Ventilation (IJV) proposed by Karimipanah and Awbi [23] forms a fresh air layer in the lower occupied zone through the collision effect between the high momentum airflow and floor, which combines the advantages of traditional MV and DV [24]. It was found that IJV had a good performance under both winter and summer conditions [25]. Wang et al. [26] and Zhang et al. [27] investigated the performances of IJV for cooling. Their results showed that the supply airflow can be consistent with the rising trend of human body thermal plume, with a corresponding high contaminant removal efficiency. For winter heating, Ye et al. [28] concluded that the removal efficiencies of CO_2 and 2.5 μm particles under IJV were higher than that under MV. With the usage of Coanda effect, Li et al. [29] proposed Wall Attachment Jet Ventilation (WAJ), which makes the air jet released from the ceiling-level inlet to be attached to the vertical wall and then move downward into the occupied zone. WAJ had been proved to have a higher ventilation efficiency than DV [30]. Yin et al. [31] investigated the law of particle movement and dispersion in the room heated by WAJ. In the case of Deflection Ventilation (DeV), it was used to deliver the fresh air into the breathing zone with help of a deflector [32-33]. Li et al. [33] numerically compared the removal effects of pathogenic microorganisms under MV, WAJ, and DeV. The results indicated that the ventilation performance of DeV was better with the action of the deflector. In a recent study, Su et al. [34] used Computational Fluid Dynamics (CFD) method and revised Wells-Riley model to calculate the infection probability in a shared office under seven

different air distribution methods in cooling mode. Their work emphasized the significant impact of air distribution method on the transmission of respiratory diseases.

1.2 Research innovations and objectives

As mentioned above, most of the previous studies focused on comparing the ventilation performances of different air distributions for summer cooling. However, due to the influence of positive thermal buoyancy, the airflow characteristics of these air distributions in heating mode can be distinct from that in summer [35, 36]. Airflow pattern is an important factor affecting particle movement, especially for fine particles. As a result, the dispersion of exhaled droplet nuclei in winter can also be different from that in summer. In addition, poor ventilation during the heating season is noted as a common phenomenon, because people often close doors and windows to reduce cold discomfort in winter. On the other hand, the statistical data of the World Health Organization (WHO) [37] and previous studies [38-41] have shown that, autumn and winter are the periods where there are known peaks of influenza activity. The air temperature and humidity conditions during this period render most respiratory viruses with lipid enveloped (such as coronaviruses, influenza, respiratory syncytial virus, etc.) so as to maintain a high survival probability in infection events [8, 39, 42-43]. Therefore, more attention should be paid to indoor air quality in winter.

This study aimed to comprehensively compare the dispersion of exhaled particles under five air distribution methods (i.e., MV, SV, DeV, IJV, and WAJ) with application potentials for the heating period. The airflow field and the spatial concentration distribution of exhaled particles were predicted using CFD. Additionally, the residence time and the fate of particles with five different diameters were also counted. The findings derived from this study is expected to provide an informed understanding of the importance of air distribution methods under heating mode, and can be helpful for the design of air distributions.

2. CFD methodology

Theory analysis [44], full-scale measurements [22], and numerical method [45] are generally used to study the movement and distribution of human exhaled pollutants. Relatively, numerical method can provide detailed flow field data, so it is widely used in enclosed spaces. In this study, the CFD numerical simulation was used, integrating the airflow as continuous phase while the exhaled particles from the infector as the discrete phase. The airflow pattern and particle dispersion were solved by Eulerian and Lagrangian methods using Fluent software, respectively.

2.1 Description of the geometry

The geometry of the model was set-up to be representative of a typical office based on a test chamber in Chongqing University. As shown in Fig. 1, the room has dimensions of 5.85 m length (X) × 5.06 m width (Y) × 2.80 m height (Z). The left wall and window are external envelopes, and other walls are internal. Two rectangular thermal manikins are set symmetrically in the space to represent the sedentary occupants. This study focuses on the effect of global air distribution on exhaled particle dispersion, so the sedentary occupant is reasonably simplified to be rectangular with dimensions of 0.4 m (X) × 0.25 m (Y) × 1.2 m (Z) [46]. The infector is highlighted and the other one is receiver, as shown in Fig. 1(b). To model the environment and the zone as close as possible to a typical office, a desk is included between the two occupants. It is noteworthy that all air distribution methods use the same physical geometry. Fig. 1(a) shows the locations of supply air inlets and exhaust outlets. The size of inlet for MV is 0.4 m × 0.2 m, which is installed on the high level of the front wall at the height of 2.42 m above floor. This location of inlet is common in real-buildings [26]. For SV, three double grilles with dimensions of 0.18 m × 0.18 m each are arranged at the middle height of the front wall [47]. In order to counteract the effect of positive thermal buoyancy on the supply air jets, the angle of the supply air jets was set as 30° downward [47], which is the same as the deflection angle of the deflector in DeV. DeV and WAJ have the identical air inlet [48], both of which supply air vertically

downward through the inlet with the size of 0.6 m × 0.18 m installed on the ceiling. The inlet of IJV is configured on the back wall and the warm airflow is supplied by an inlet at the height of 0.8 m above floor, with a cross-sectional area of 0.5 m × 0.25 m [23]. Two same outlets with dimensions of 0.2 m × 0.4 m each are applied for all five air distributions. The better indoor air quality can be achieved by setting the exhaust outlets on the ceiling [49]. For all cases, the supply inlets provide 100% full fresh air.

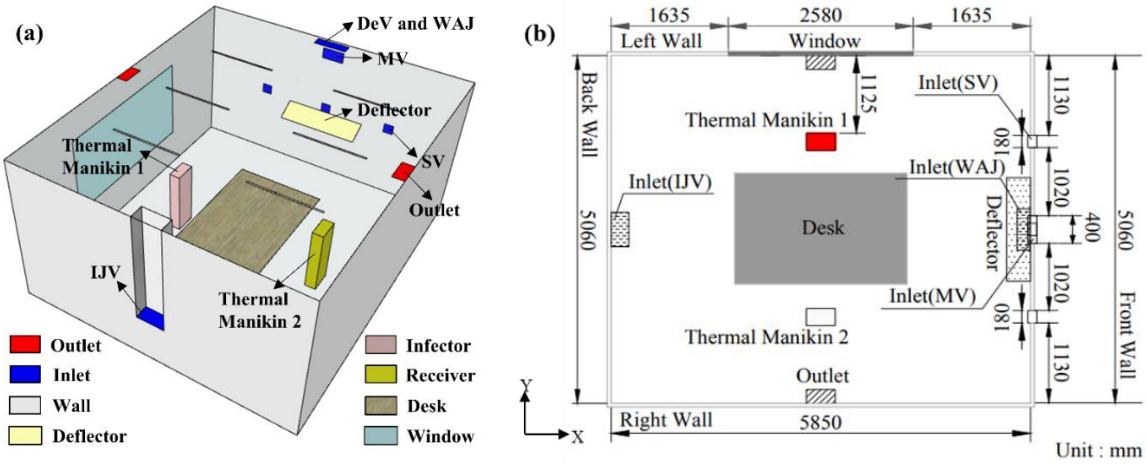

Fig. 1. Typical office room, (a) illustration of the setup of the office model (supply air inlets and exhaust outlets for different air distributions); (b) plan view of the office room.

2.2 Numerical method

2.2.1 Airflow phase simulation

Turbulent airflow is a highly non-linear and complex physical phenomena, and the standard k-ε turbulence model (k and ε are turbulent kinetic energy and turbulent dissipation rate, respectively) was employed in this study to solve it. This model is an ideal compromise between the accuracy and computational cost, which is widely validated by the previous studies focused on enclosed environments [50-52]. The general governing equation of steady flow is written as follows [50].

$$\frac{\partial(\rho u_i \emptyset)}{\partial x_i} = \frac{\partial}{\partial x_i}\left(\Gamma_\emptyset \frac{\partial \emptyset}{\partial x_i}\right) + S_\emptyset \quad (1)$$

Where ρ is density (kg/m^3); u_i represents the velocity in i direction; $\Gamma_\emptyset$ is the effective diffusion coefficient; $S_\emptyset$ is the source term. More details about the governing equations and the turbulence parameters of the standard *k*-ε model can be found in the research of Zhai et al. [50].

To maintain the quality of CFD prediction, the governing equations were discretized using second-order upwind schemes [51]. The finite volume method and Semi-Implicit Pressure Linked Equation (SIMPLE) algorithm were employed for discretization and to solve the Navier-Stokes equations, respectively. The airflow changes greatly due to the steep air velocity or temperature gradients near the vents, heat sources, and walls, so the grid was refined in these areas. Meanwhile, in order to improve the calculation accuracy in near-wall regions, the average wall y^+ value was kept less than 5, and the enhanced wall function was adopted [53]. Boussinesq model was set to consider the buoyancy effect. The radiation heat transfer was calculated by Discrete Ordinates (DO) radiation model [54]. The solutions were considered to obtain convergence when the residual values were less than 10^{-5}, the energy and DO equations were concurrently less than 10^{-6}.

2.2.2 Particle phase simulation

For steady environments, both Eulerian method [7, 18, 55] and Lagrangian method [26, 56-57] can be used to predict the transport of particles well. Considering the low particle load (i.e., the volume fraction of discrete phase is less than 10% of the room volume), the Lagrangian method was considered appropriate [58]. The movement of particle is described by Newton's second law (Equations 2 and 3):

$$\frac{du_{pi}}{dt} = F_i \quad (2)$$

$$F_i = \frac{18\mu C_D Re}{24\rho_p d_p^2}\left(u_i - u_{pi}\right) + g\left(1 - \frac{\rho}{\rho_p}\right) + F_{ai} \quad (3)$$

Where subscripts i, p denote direction and particle, respectively; u is velocity (m/s); F is force on the particle of per unit mass (m/s^2); μ is the molecular viscosity of air (kg/(m·s)); ρ is density (kg/m^3); d_p is particle diameter (m); g is gravitational acceleration constant (m/s^2); Re is Reynolds number; F_{ai} is the additional force exerted on the particle of per unit mass (m/s^2); and C_D is drag coeffcient, which can be written as follows:

$$C_D = a_1 + \frac{a_2}{Re} + \frac{a_3}{Re^2} \tag{4}$$

Where a_1, a_2, and a_3 are constants [16].

For Eq. (3), the first item on the right ($\frac{18\mu C_D Re}{24\rho_p d_p^2}(u_i - u_{pi})$) represents the drag force between the particle and surrounding air; the second term ($g\left(1 - \frac{\rho}{\rho_p}\right)$) represents the gravity of the particle itself; and the third item (F_{ai}) represents the additional forces. In this study, three additional forces were considered to be exerted on the particles: (i) Brownian force, which is closely related to the dispersion behavior of small-sized particles; (ii) Saffman lift force, which is caused by the velocity gradient in indoor airflow field; and (iii) Thermophoresis force, due to the non-isothermal flow condition, particles are driven to the direction of low temperature under the gradient. Detailed formulas for calculating these forces can be found the research of Zhao et al. [16].

The pulsation airflow breathed from the mouth develops into turbulence when it is a short distance away from the mouth [44]. Thus, the complicated process of particles production caused by breathing was simplified to be released from the mouth (a rectangular with the size of 0.02 m × 0.01 m [18]) with a constant rate. In order to distribute the effect of discrete phase evenly across neighboring cells (adjacent cells share at least one grid node with cells whose trajectories intersect), the option of "Enable Node Based Averaging" was checked [53]. The instantaneous turbulent velocity has a significant effect on particle trajectory. In this study, the instantaneous velocity of the particle was expressed by Gaussian random distribution. The discrete random walk (DRW) model was

introduced to define velocity fluctuation as Gaussian distribution and to simulate the stochastic behavior of particles caused by turbulence fluctuation, as follows:

$$u_a^{'} = \Phi \sqrt{u_a^{'}} = \Phi\sqrt{2k/3} \quad (5)$$

Where $u_a^{'}$ is fluctuating component of air velocity; k is turbulent kinetic energy; and Φ is normal distribution random number.

2.3 Boundary conditions

For purpose of comparison, considering the indoor heat load and the requirement of outdoor fresh air, the ventilation rate of the five air distributions in this study was 423 m^3/h. The air changes per hour (ACH) was 7.0 accordingly. The supply air is free of particles. The supply air inlet was set as velocity inlet boundary condition with a temperature of 24 °C for all five air distribution methods, and the outlet was set as outflow boundary condition. The heat sources in the office include two manikins and six fluorescent lamps, with the generated heat of 100 W per person and 23 W per lamp. The window-to-wall ratio is 0.26 for the exterior wall and window. Considering the fact that outdoor air temperature typically varies from 2.2 to 10 °C in winter in Chongqing [59], the limited values of 0.8 and 3.0 W/(m^2·K) for heat transfer coefficient (K) of exterior wall and window specified in the Chinese National Standard GB 50189-2015 [60], the interior surface temperatures of the exterior wall and window were set at 15 and 13 °C, respectively. Other walls were treated as adiabatic. All the surfaces were modeled as non-slipped. The boundary conditions for the airflow phase are summarized in Table 1. For the cases of this study, the initial Reynolds numbers (Re) of the five air distributions were in the range of 22,000 – 43,000, and the Archimedes numbers (Ar) were in the range of 0.005 – 0.02.

Table 1. Boundary condition settings for airflow phase

Type	Boundary condition
Air supply	Supply air temperature is 24 °C for all five air distribution methods The ACH value is 7.0 for all five air distribution methods
Air exhaust	Outflow
Lamps	Constant heat flux of 639 W/m^2
Manikins	Constant heat flux of 62.5 W/m^2
Left wall	Constant temperature of 15 °C
Window	Constant temperature of 13 °C
Other walls	Adiabatic

The particle dispersion was modeled using the discrete phase model (DPM). The infectious exhaled droplet nuclei can be regarded as the inert particle, which was injected out from the mouth with a constant velocity of 0.5 m/s [18]. The pulmonary ventilation volume rate of the injector was set at 6 L/min for light office work [61]. The temperature of exhale air was 35 °C [62], standing for the neutral temperature of human body. The dispersion characteristic of submicron particles is similar to that of tracer gas [55]. For coarse particles ($d \geq 50$ μm), the influence of airflow on particle dispersion is minor, and the airflow cannot effectively remove these coarse particles [26, 57]. According to a review by Mao et al. [63] on the number distribution and the cumulative volume of exhaled droplets from different respiratory activities, five typical particle diameters of 1, 5, 10, 30, and 50 μm were therefore chosen for this study. The density of particles was 1006 kg/m^3, slightly larger than water [64]. For all solid surfaces, the “trap” condition was applied to reproduce the deposition of particles, while the “escape” boundary condition was set for the air inlets and outlets. This means that the particle trajectory calculation is terminated when the particle reaches surfaces of walls or vents. The boundary conditions of the discrete phase are listed in Table 2.

Some assumptions were made for the numerical simulation of the discrete phase in this study. Firstly, due to the low volume fraction of exhaled particles, the two–phases interaction was considered as a one-way coupling. The effects of the particles on indoor airflow were ignored [26]. Secondly, the breathing airflow developed into turbulence after moving for a short distance [44]. This study focuses on the dispersion of exhaled particles in the office. Thus, the periodic breathing of thermal manikin was simplified as exhalation with a constant rate [26]. Thirdly, for droplets with a diameter of less than 100 μm, the time of the transient process from a droplet to a droplet nucleus due to evaporation was fairly short [65], so the evaporation effect of droplets was neglected. Finally, the heat transfer between indoor air and the exhaled particles was also neglected.

Table 2. Boundary condition settings for the discrete phase

Type	Boundary condition
Mouth	Velocity-inlet (v = 0.5 m/s) The temperature of exhaled flow is 35 °C The pulmonary ventilation volume rate is 6 L/min
Particle sizes	1, 5, 10, 30, and 50 μm
Particle density	1006 kg/m^3
Walls	Trap
Inlets	Escape
Outlets	Escape

2.4 Grid-independent tests

The structured hexahedral grids were applied to the computational domains using ICEM, a component within the ANSYS CFD software. Since all surfaces in the simulated chamber are

rectangular, the hexahedral grid type was chosen to reduce the number of cells and improve the computational accuracy and efficiency. To further improve the reliability of results, local refinements had been made around locations where air velocity or temperature gradient was relatively steep. The refined first layer of grid was 6 mm thickness and the growth rate was kept between 1.01 and 1.35, with a maximum cell width of 90 mm to guarantee the aspect ratio of cells less than 15. To ensure the independence of mesh solution, each air distribution was checked by four different mesh numbers. Taking DeV as an example, four numbers of mesh grids (i.e., 2.45 million, 4.11 million, 5.77 million, and 7.45 million) were generated for the grid-independent tests. As shown in Fig. 2, by comparing the air temperature and air velocity distributions at the vertical centerline of the room (X = 2.925 m, Y = 2.53 m), the grid number of 5.77 million was selected with a consideration of computational accuracy and cost. Fig. 3 shows the strategies of mesh generating for two cross sections in the middle of the office (X = 2.925 m and Y = 2.53 m) served by DeV. The details about the ultimate mesh number for the five air distribution methods are listed in Table 3.

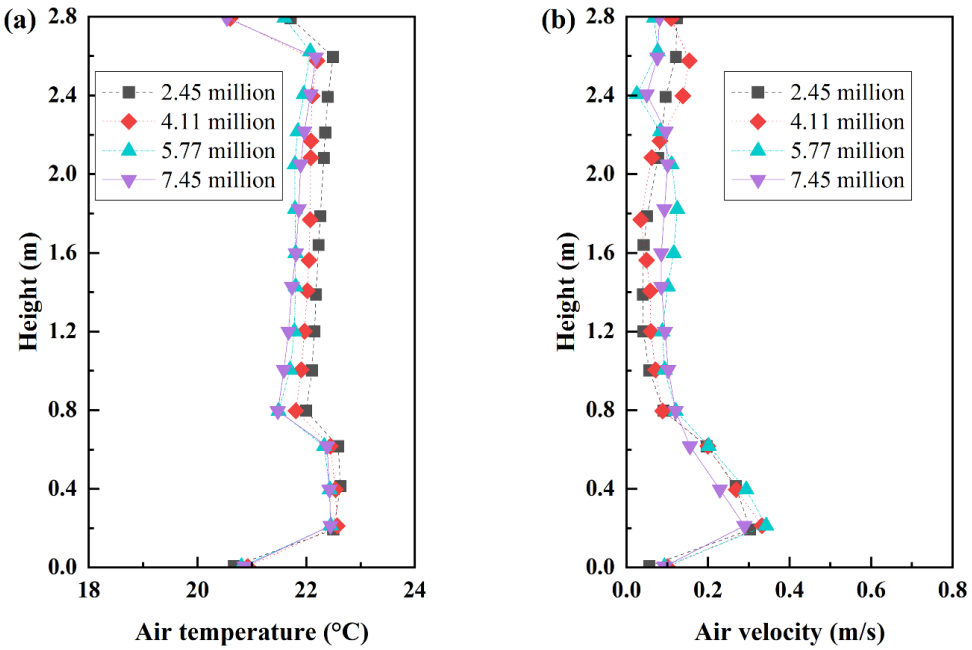

Fig. 2. Comparison of predictions using four levels of mesh grids. (a) air temperature; (b) air velocity.

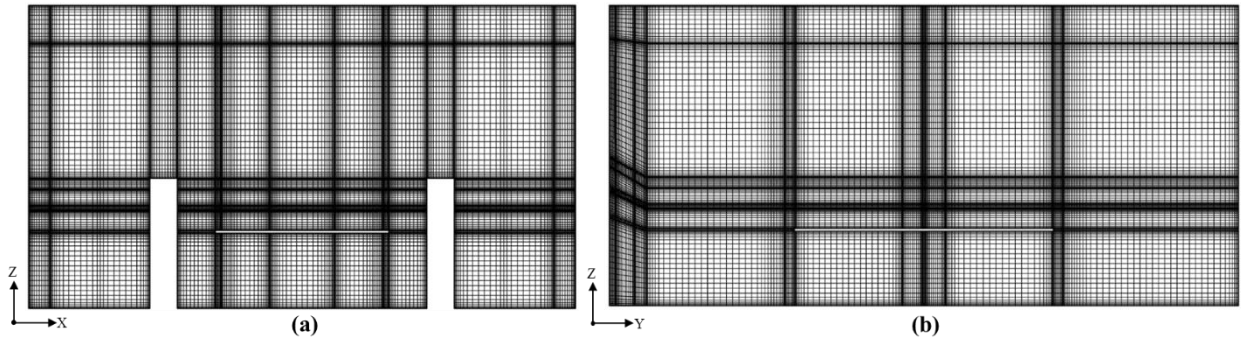

Fig. 3. Meshes for Deflection Ventilation (DeV). (a) X = 2.925 m, and (b) Y = 2.53 m.

Table 3. Grid details with different air distributions

Method	Growth ratio	Non-dimensional wall distance, y^+	Number of elements
MV	1.15 – 1.35	4.20	5,385,587
SV	1.20 – 1.35	4.04	6,013,748
DeV	1.15 – 1.35	3.68	5,771,292
IJV	1.10 – 1.35	4.18	5,501,705
WAJ	1.10 – 1.35	4.12	5,303,231

The Lagrangian technique is a stochastic method. The more trajectories there are, the more stable the solution is. To avoid statistical distortion, a sensitivity analysis of the number of injected particles is required. In this study, four different particle numbers (i.e., 10,000, 20,000, 30,000, and 40,000) were selected and checked. As shown in Fig. 4, when the absolute deviations of suspension rate, deposition rate, and removal rate of particles were less than 1% concurrently compared with the case having the largest number of particles, the statistics were considered as accurate. As a result, a suitable number of injected particles was assigned to be 20,000 in this study.

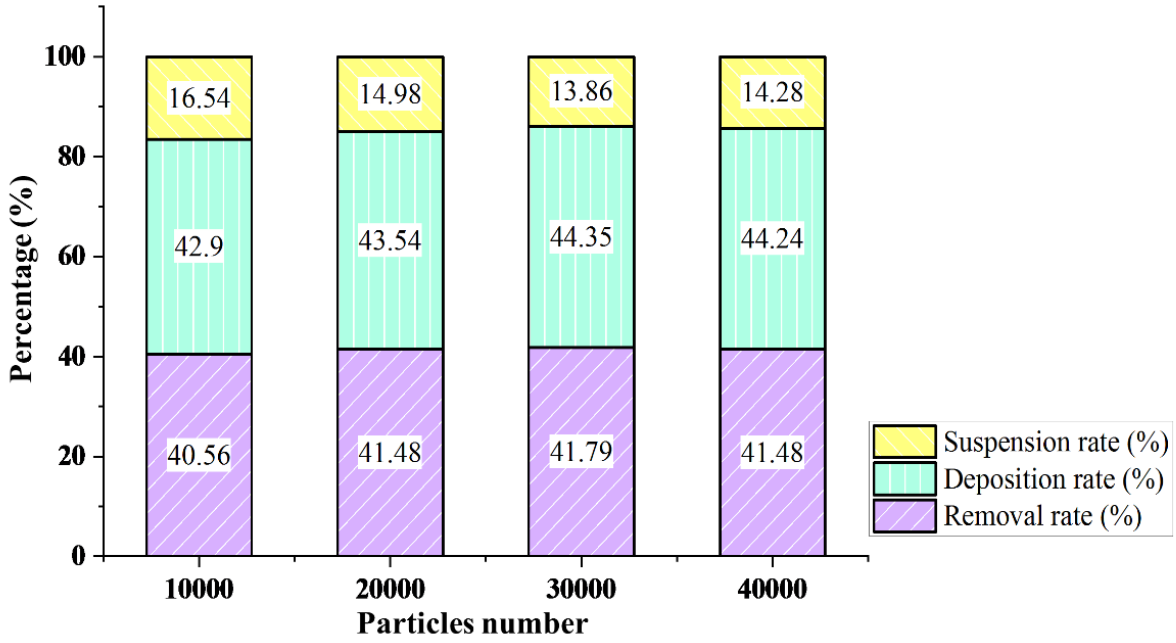

Fig. 4. Comparison of predictions using different particle numbers.

2.5 Validation for numerical models

2.5.1 Validation for airflow model

A prerequisite for simulating indoor airflow fields is the proper selection of turbulence modeling method. Previous studies showed that the standard *k*-*ε* model can be used to accurately predict air flows under different air distributions. For SV, Cheng [66] found that the standard *k*-*ε* model slightly better predicted the air velocities and temperatures than RNG *k*-*ε* model and SST *k*-*ω* model. The standard *k*-*ε* was also applied for the numerical analysis of indoor air quality under SV, DV, and MV [67]. For IJV, Zhang et al. [27] compared the prediction results of the standard *k*-*ε* model with the experimental data, and the results showed that this model can provide satisfactory accuracy. For WAJ, the standard *k*-*ε* and RNG *k*-*ε* models presented similar prediction accuracy, and all the results were acceptable [68].

To validate the simulation accuracy of standard *k*-*ε* model for DeV, we carried out the experiments in a full-scale climate chamber located at Chongqing University. This chamber is

identical with the dimensions of the geometry model in this study (see Fig. 1). The supply airflow rate was set at 5.5 ACH, and the air supply temperature was 24 °C. The deflection angle of the deflector was adjusted to 35° downward. The warm air was discharged from a rectangular inlet with the size of 0.58 m × 0.18 m on the ceiling, and indoor air was exhausted by an outlet with the size of 0.56 m × 0.26 m at the bottom of the opposite wall. The heat sources consisted of thermal manikins and lamps, and their arrangement is symmetrical, as seen in Fig. 5(a). The interior surface temperatures of all envelopes were collected by automated thermal recorders (WZY-1) at a frequency of 60 Hz. The error of the instruments within the measurement range of -20 – 80 °C was ± 0.5 °C. As shown in Fig. 5(a), three typical plumb sampling lines (L1 – L3) were arranged around the airflow route and manikins to collect the air temperature and velocity at the heights of 0.1, 0.6, 1.1, 1.7, and 2.4 m above floor. The data acquisition systems used the Swema 03+ omnidirectional anemometers, which have the measurement accuracy of ± 0.03 m/s ± 3% of readings in the range of 0.05 – 10 m/s and an accuracy of ± 0.2 °C in the range of 10 – 40 °C. Data were collected after the airflow field reached stability. The repeated experiments were also carried out to verify the measured results. The relative deviations of the measured parameters were less than 10%, showing that the measured results were reliable.

The measured air velocities and air temperatures along three sampling lines were compared with the corresponding predictions by the standard k-ε model, and the results are shown in Fig. 5(b). A slightly larger discrepancies can be observed along Sampling Line L1. This may be due to the instability of experimental conditions due to the variation of outdoor weather. Additionally, the airflow near the deflector is more complex and more difficult to be predicted accurately. In this study, the Root Mean Square Error (RMSE) and Mean Absolute Error (MAE) were used to quantify the difference between the simulation results and experimental data. For air velocity, the RMSE and MAE were 0.046 and 0.041 respectively. For air temperature, the RMSE and MAE were 0.659 and

0.632 respectively. Moreover, the simulation results exhibit the similar variation trend with the experimental data. Therefore, it is considered that the simulated air velocity and temperature agree well with the measured results, and the standard *k-ε* model can be reliably used to predict the air flows under DeV.

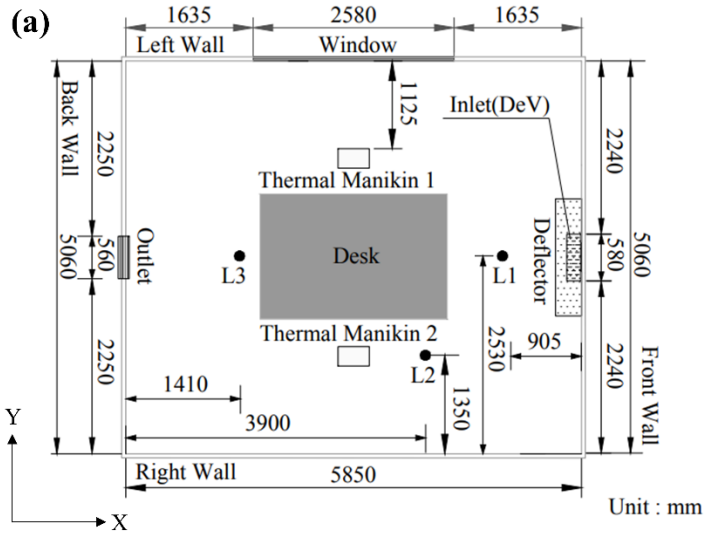

Note: L1 – L3 are three typical sampling lines in the chamber.

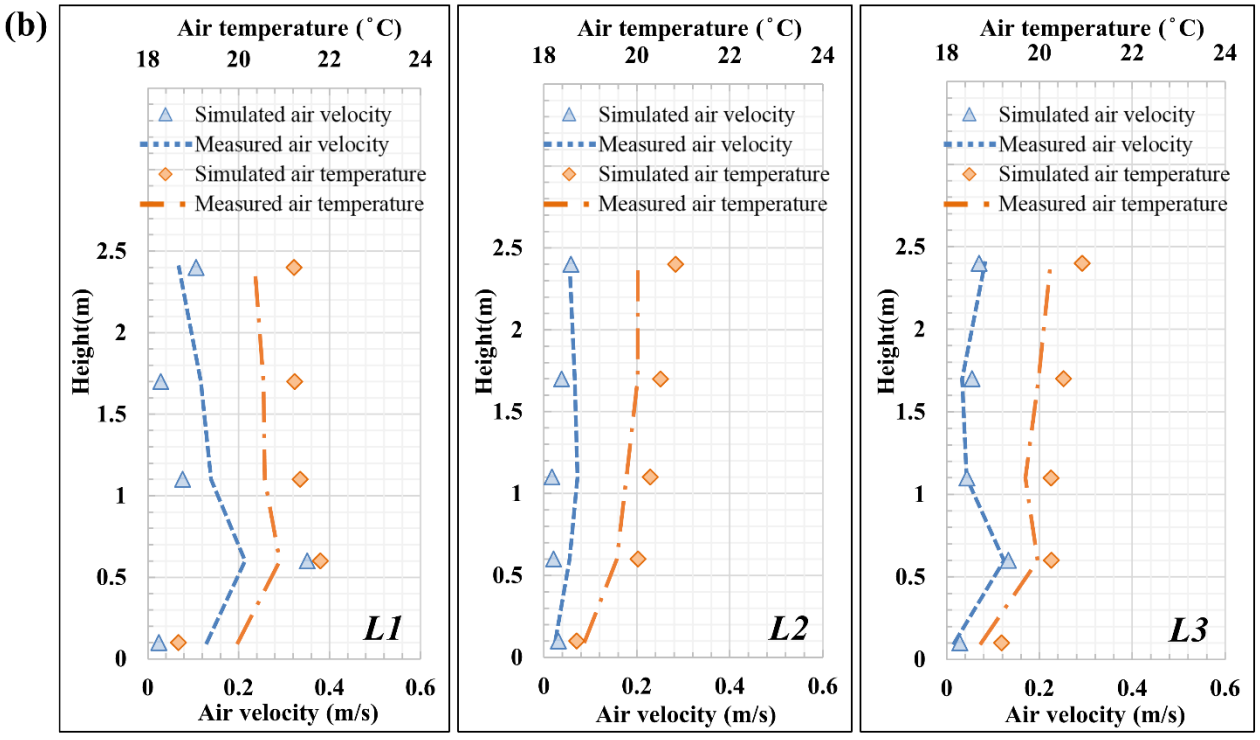

Fig. 5. (a) Schematic plan of the test chamber layout; (b) Comparisons of air velocity and temperature between CFD simulations and experiments along Sampling Lines L1 – L3.

2.5.2 Validation for particle transport model

The validation of particle transport model was on the basis of the experimental results reported by Chen et al. [69]. For the experiment, spherical particles were injected into the chamber from a supply air inlet with a speed of 0.225 m/s. The average particle diameter was 10 μm and the density of all particles was 1400 kg/m^3. By the phase Doppler anemometer system, they obtained the stable particle concentration in the chamber. The boundary conditions can be found in the research of Chen et al. [69]. The plan of the chamber layout and sampling lines is schematically presented in Fig. 6(a).

The experimental data from the literature were used for validation. A comparison of the particle concentrations along three sampling lines between the predictions by Lagrangian method and the measurements is shown in Fig. 6(b). The average relative error of the normalized particle concentrations for all measurement points is 9.1%, showing that the predicted concentrations correspond well to the experimental data. This indicates that the Lagrangian model can reasonably predict indoor particle dispersion. Thus, the Lagrangian method can be used for further investigations.

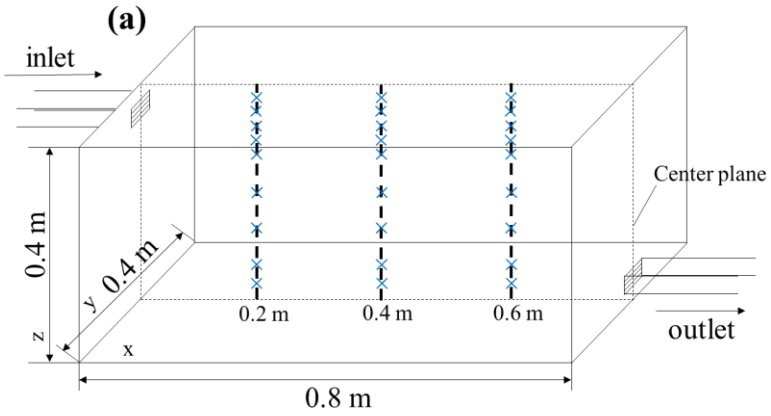

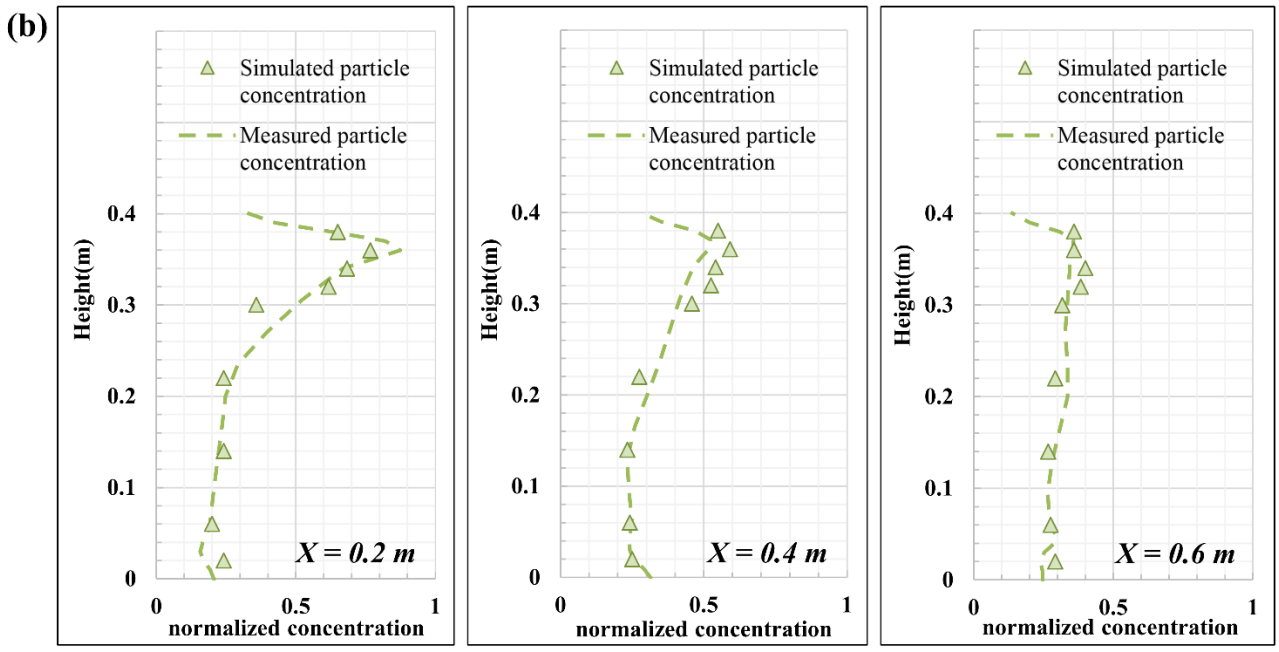

Fig. 6. (a) Geometry model of the ventilation chamber [69]; (b) Comparison of the simulated particle concentration with experimental data.

3. Results

3.1 Airflow field

Fig. 7 presents the distributions of air temperature and air velocity on the representative cross-section (Y = 2.53 m). The air temperatures in the occupied zones under all scenarios remain between 19.3 and 23.5 °C, and the vertical air temperature differences between the head and ankles were less than 2 °C, meeting the requirements of thermal comfort [70]. However, it was seen that air distribution methods significantly affected indoor airflow pattern.

For MV, the warm supply airflow did not effectively enter in the occupied zone because of the effect of positive thermal buoyancy. The indoor air temperature stratification was evident. The vertical air temperature difference between the upper and lower zones in the room was larger than 3°C. As observed in Fig. 7, the air velocity in the occupied zone was low, generally below 0.1 m/s.

The air velocity decayed fast along the right wall, because of the positive thermal buoyancy in the opposite direction. As a result, a large recirculation zone was formed near the right wall.

For SV, the warm airflow was forced to be transported directly to the occupant from the inlets on the side wall. For DeV, the warm airflow was guided into the occupied zone after the deflection effect of the deflector. Under the action of thermal buoyancy, the supply airflows started to rise after a certain distance. In addition, the air temperature distributions of SV and DeV were similar and the air temperatures in the occupied zone exceeded 21 °C. This means that the supply airflow is efficiently delivered to the occupied zone [71]. However, some differences can be observed for their air velocity distributions. Compared with DeV, the air velocity under SV was higher in the occupied zone, which can be attributed to the fact that the supply air inlets of SV were closer to the occupied zone.

For IJV and WAJ, the air temperatures at the floor level near the supply air jet zone were high, exceeding 22 °C. The air lake can be observed at the bottom of the room. However, the distance of supply air jet penetration was short, and the range of air lake formed was small. This was the result of the influence of positive thermal buoyancy on supply airflow under heating mode. In addition, the airflow pattern in the occupied zone of IJV and WAJ showed some similarities, but the penetration length of the airflow attached to the floor was longer and the size of air lake was larger in the room with IJV. This is because the distance between the inlet of IJV and the floor is shorter, and the supply airflow maintains a higher momentum in the occupied zone. It could be seen that two recirculation zones were formed near the occupants in the rooms served by IJV and WAJ, which was attributed to the blocking effect of the desk. Regarding IJV, the range of the recirculation zone was larger, and its impact on the exhaled particle removal may be greater. This will be further analyzed in Section 3.2.4.

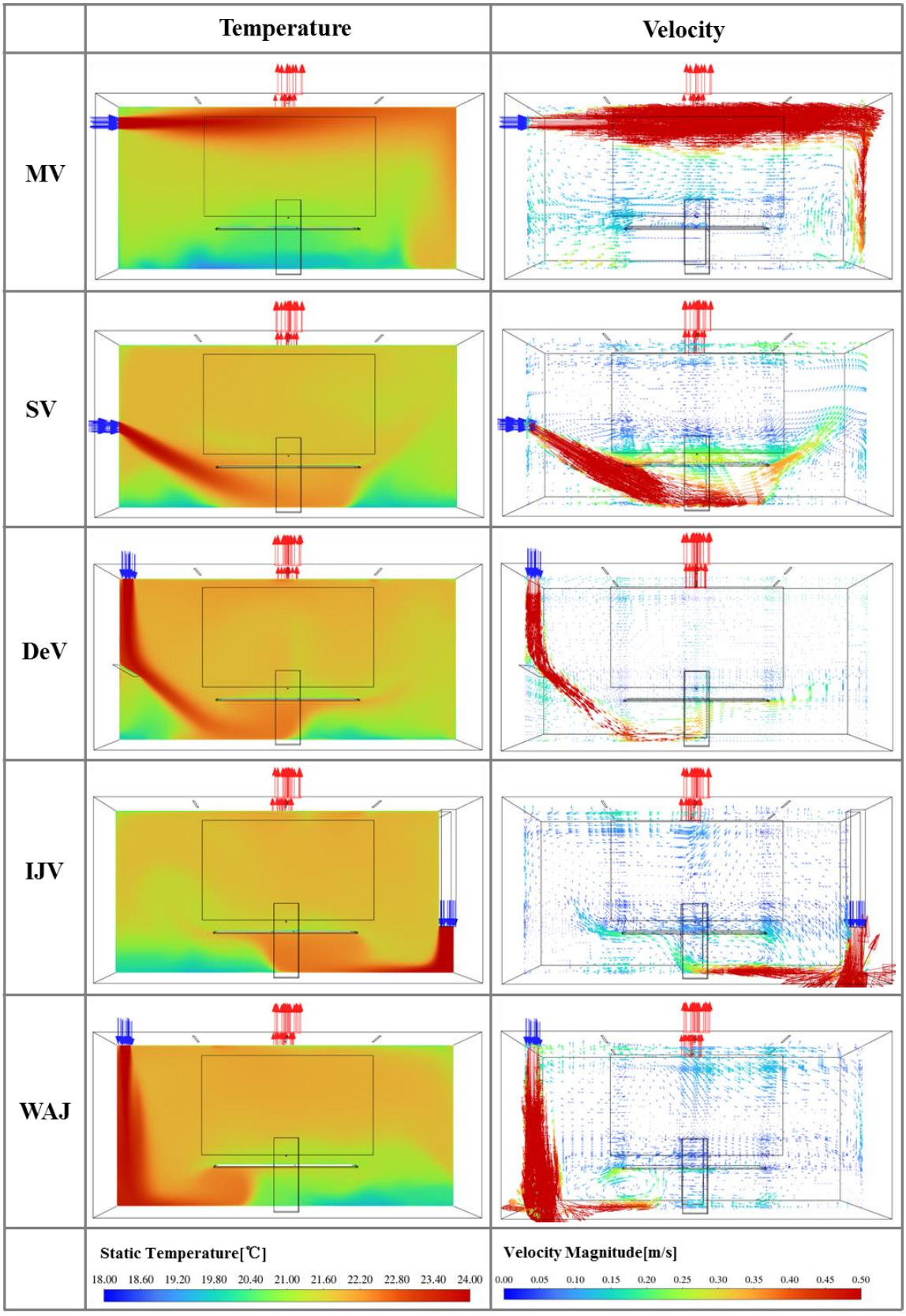

Fig. 7. Distributions of air temperature and air velocity in the middle section (Y = 2.53 m) of the

room under different air distributions.

Fig. 8 shows air temperature profiles of the rooms served by five different air distribution methods. It could be seen that indoor thermal stratification under MV was the most evident. The air temperature difference from the floor to the ceiling reached 3.4 °C, and the vertical air temperature gradient was 1.3 °C/m. The air temperature almost increased linearly along the height of the room. As mentioned above, this indicated that a smaller amount of warm supply airflow entered the occupied zone due to the influence of positive thermal buoyancy. For SV, DeV, IJV, and WAJ, the air temperatures in the upper zone were similar, fluctuated between 21 and 22 °C. The air temperatures at the lower zone of the room served by DeV, IJV, and SV were slightly higher, indicating that these air distributions can transport more heat energy and fresh air to the occupied zone.

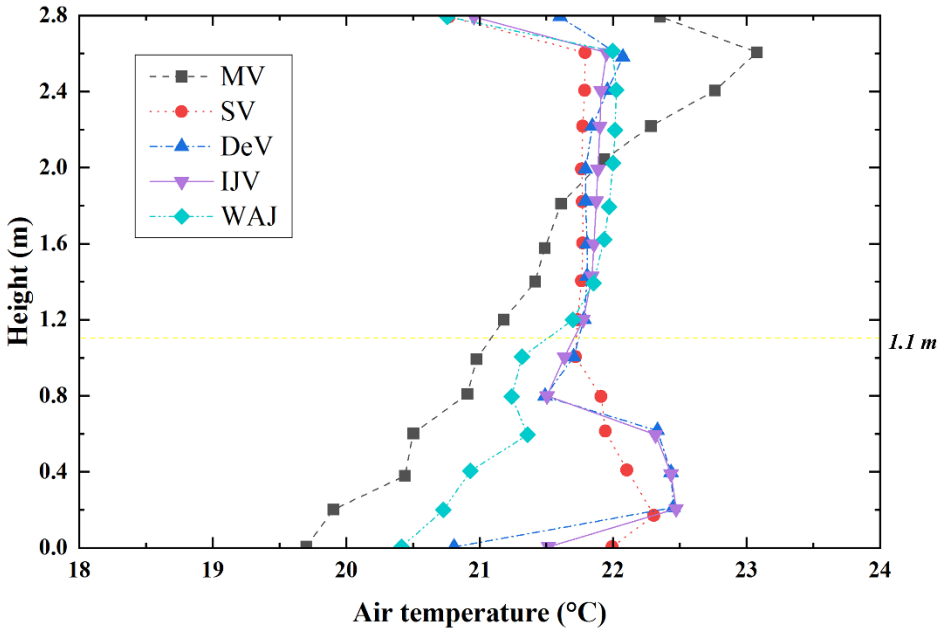

Fig. 8. Air temperature profiles of the rooms served by different air distribution methods.

3.2 Diffusion and distribution characteristics of particles

3.2.1 Normalized concentration distribution

To compare the spatial particle concentration distribution intuitively, a Custom Field Function (CFF) was established for each case. The indoor particle concentration was normalized using the average particle concentration at the two exhausts under five air distribution methods. Fig. 9 shows the results of normalized concentration distributions of exhaled particles. Due to the different airflow fields under five air distribution methods, some differences in their particle concentration distributions were found.

For MV, the particle concentration at the vicinity of infector exceeded 5 times of the exhaust outlets. This is because the air velocity around the infector is low and the control effect of supply airflow on the exhaled particles is weak. Moreover, the concentration distributions showed that some particles moved to the area near the supply opening, which might be affected by the entrainment effect of the supply air jet. At the breathing zone (i.e., Z = 1.1 m), the average normalized particle concentration was 4.45, and the contour indicated that the exhaled particles could spread along the horizontal direction to reach the microenvironment of the opposite occupant. This means that the fresh air rarely spreads over the occupied zone and does not dilute the particle concentration effectively, which is caused by the negative influence of thermal buoyancy on supply airflow.

For SV, DeV, IJV, and WAJ, the high concentration region can be clearly observed above the infector. This indicated that the airflow would be enough to control the movement of exhaled particles when it reached the occupant. However, the particle concentrations were relatively higher in other regions of the room under IJV and WAJ, showing that both SV and DeV had the stronger control effect on the exhaled particles. On the one hand, this may be due to the higher air velocities under SV and DeV at the microenvironment of the occupant. Furthermore, the blocking effect of the desk and the recirculation zones formed under IJV and WAJ also have the significant impact on the

concentration distribution. At the breathing zone, the average normalized particle concentration under IJV and WAJ were 1.36 and 1.41 respectively, indicating that IJV and WAJ were more advantageous than MV (i.e., normalized particle concentration at the breathing zone = 4.45). For SV and DeV, the average normalized particle concentrations at the breathing zone were 0.56 and 0.67 respectively, showing a lower risk of cross infection in the occupied zone. Thus, SV and DeV had the higher ventilation efficiency for heating.

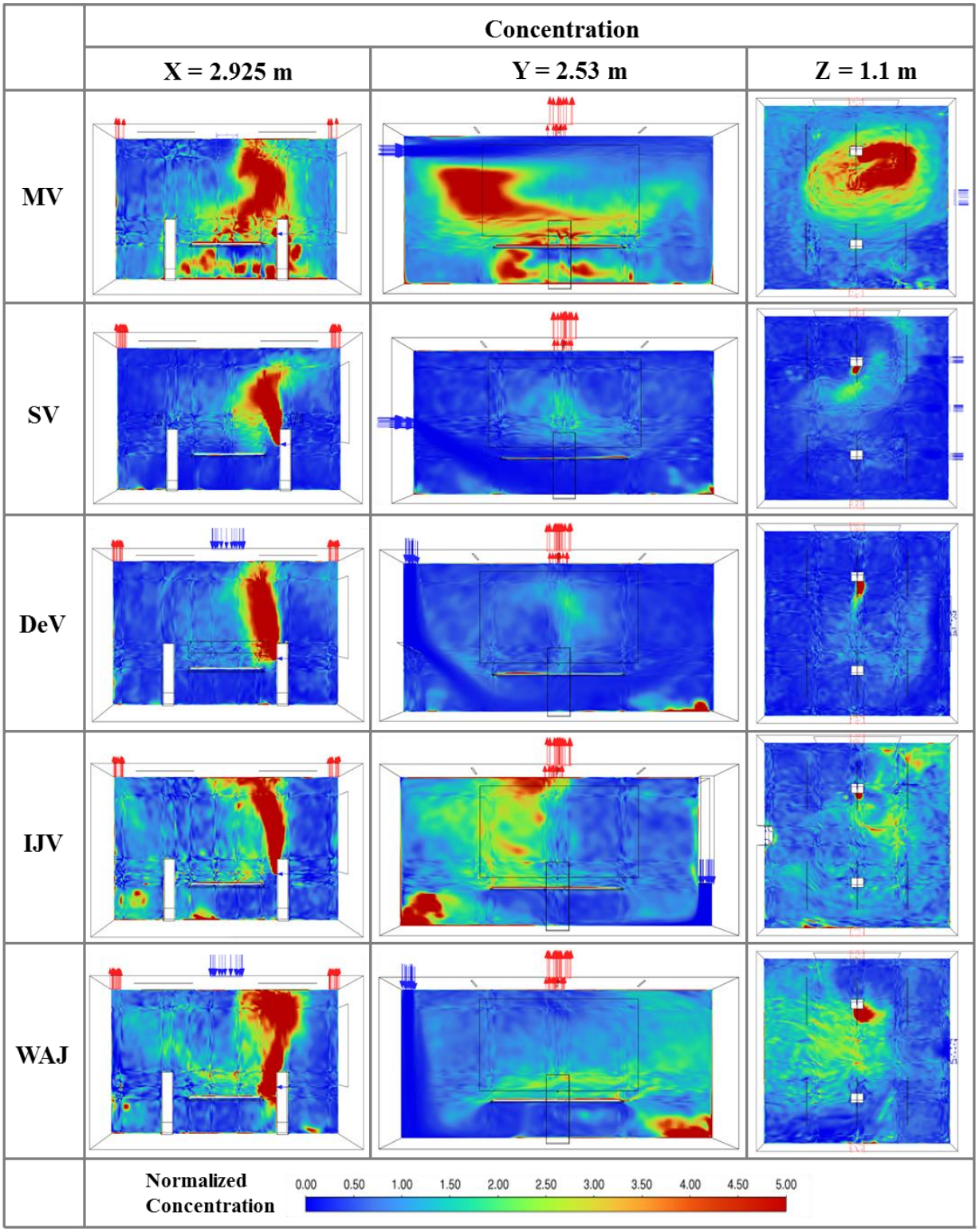

Fig. 9. Normalized particle concentrations in two middle sections (X = 2.925 m; Y = 2.53 m) and at the breathing zone (Z = 1.1 m).

3.2.2 Particle residence time

Fig. 10 shows the residence time of the injected particles in the office. The order numbers a-e represent the five air distribution methods of MV, SV, DeV, IJV, and WAJ, respectively. The order numbers 1 and 2 represent two typical particle sizes respectively: 1 – fine particles (diameter = 5 μm), and 2 – coarse particles (diameter = 50 μm). The larger the particle residence time, the longer it takes for the particles to leave the room, increasing the risk of virus transmissions of infectious diseases.

In all cases, the initial conditions of the particle release are identical. Under the five air distribution methods, Figs. 10 (a1) – (e1) illustrate that fine particles generally exhibit longer lifetimes, with the residence time more than 300 seconds. Thus, the fine particles could be transmitted for long-distance dispersion by following air flows. However, for the coarse particle, the effect of gravity was significant. Similar to the results of previous studies [57], the coarse particles had a shorter residence time in all cases (see Figs. 10 (a2) – (e2)). The residence times of the coarse particles were less than 90 seconds in the room, suggesting that they were difficult to suspend in the air for long time. Therein, the coarse particles in the room with MV disappeared fastest, which only stayed near the infector for a short moment (less than 30 seconds), as shown in Fig. 10 (a2). This phenomenon illustrates that the supply airflow had a negligible effect on the coarse particle dispersion under MV for heating mode. For SV, DeV, IJV, and WAJ, as shown in Figs. 10 (b2) – (e2), the coarse particle with diameter of 50 μm can be affected by room airflows and moved upward. Besides, due to the higher air velocity in the room with SV, the coarse particles moved backwards, which could prevent particles carrying the virus from entering the inhalation region of the opposite receiver directly.

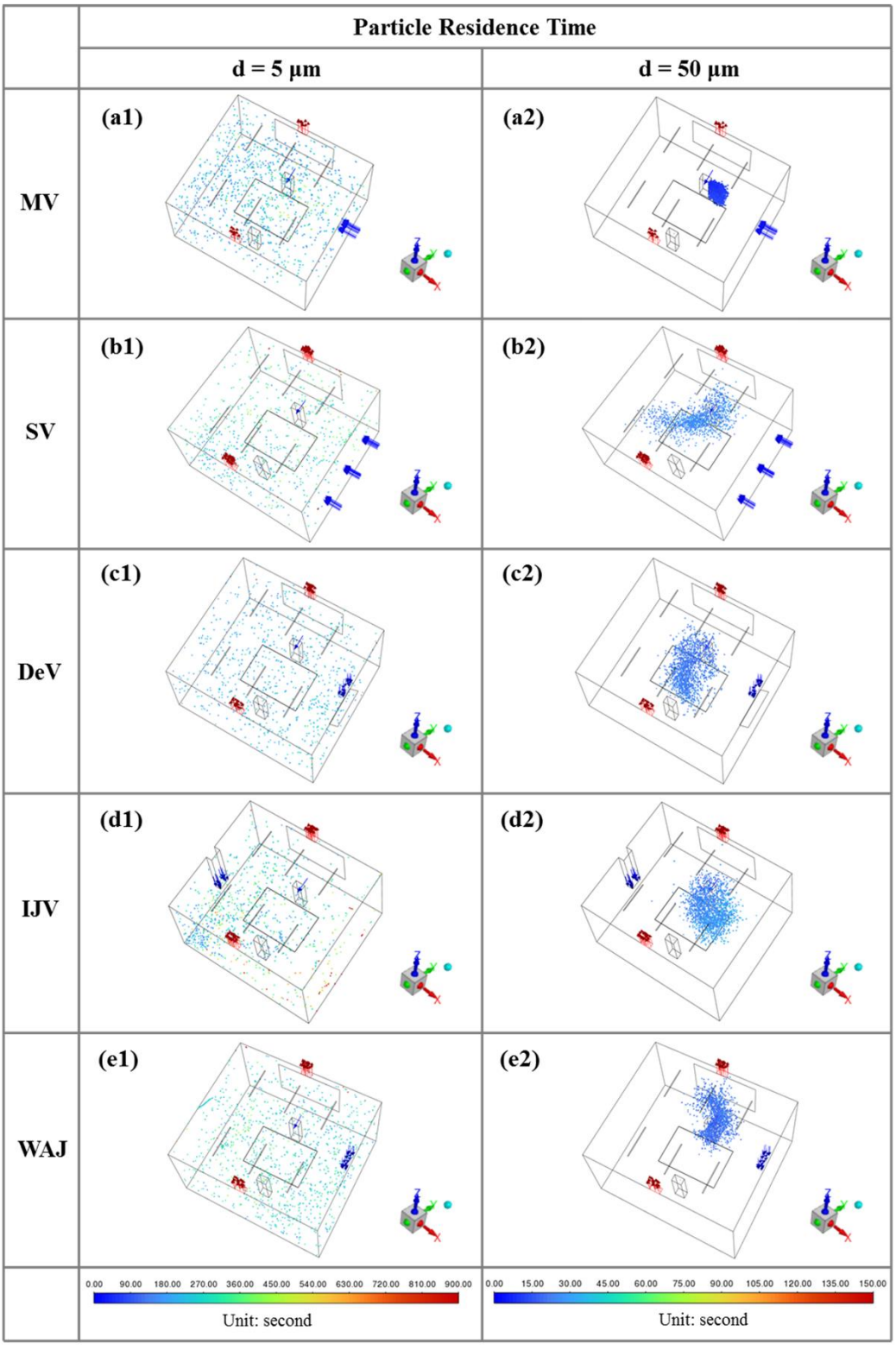

Fig. 10. Residence time of particles with two typical diameters (5 and 50 μm) under different air distribution methods.

3.2.3 Deposition rate statistics

The deposition fractions of exhaled particles with different particle sizes are presented in Fig. 11. The deposition fraction is defined as the ratio of the number of particles depositing on a certain surface to the total number of particles released from the infector.

For fine particles (diameter ≤ 10 μm), Figs. 11 (a) – (c) illustrate that air distribution methods have a significant influence on their depositions. For MV, SV, DeV, IJV, and WAJ, the average deposition fractions of fine particles with three sizes studied were 44.61%, 31.42%, 17.32%, 28.85%, and 20.51% respectively. A higher deposition fraction was found for MV, which might be caused by the following reasons. Firstly, the air velocity in the occupied zone of the room with MV was low, and the particles tended to disperse and deposit freely. Secondly, a large recirculation zone was formed near the wall, increasing the probability of fine particles to contact with walls. As a result, a higher deposition fraction was found for the walls than those for other solid surfaces. In addition, the results showed that no matter which air distribution method was applied, the deposition fraction of fine particles did not change significantly with the increase of the particle size from 1 μm to 10 μm, and the fluctuation was kept within 10%. This indicated that for fine particles, the influence of gravity can be neglected.

Figs. 11 (d) – (e) present the percentages of particles depositing on different surfaces of the room when the particle sizes are 30 and 50 μm, respectively. As expected, the major factor affecting the deposition of coarse particles was its own gravity. Thus, the deposition fraction on the horizontal surfaces (e.g., the floor and desk) increased markedly. The results showed that the deposition fraction on the horizontal surfaces in all cases accounted for more than 60% when the particle diameter exceeded 30 μm, indicating that the gravity of the particle could overcome the drag force from airflow after the particle reached a certain critical diameter. This means that the control of particles by air distributions was no longer dominant for this instance.

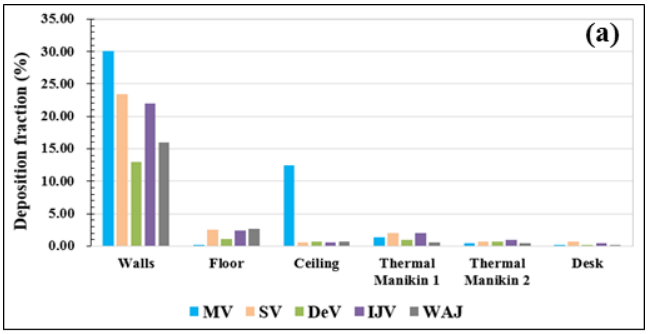
(a)
Deposition fraction (%)
35.00
30.00
25.00
20.00
15.00
10.00
5.00
0.00
Walls
Floor
Ceiling
Thermal Manikin 1
Thermal Manikin 2
Desk
MV
SV
DeV
IJV
WAJ

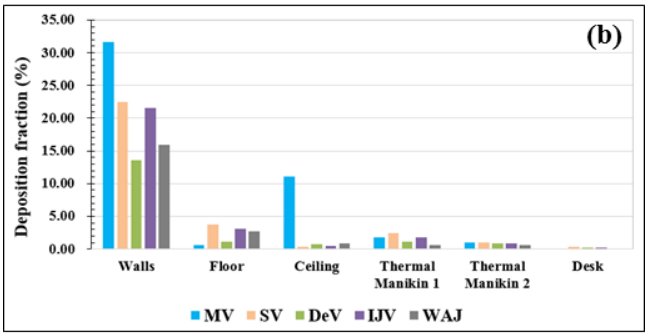
(b)
Deposition fraction (%)
35.00
30.00
25.00
20.00
15.00
10.00
5.00
0.00
Walls
Floor
Ceiling
Thermal Manikin 1
Thermal Manikin 2
Desk
MV
SV
DeV
IJV
WAJ

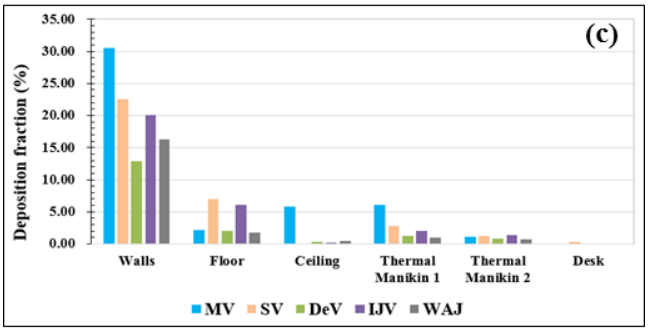
(c)
Deposition fraction (%)
35.00
30.00
25.00
20.00
15.00
10.00
5.00
0.00
Walls
Floor
Ceiling
Thermal Manikin 1
Thermal Manikin 2
Desk
MV
SV
DeV
IJV
WAJ

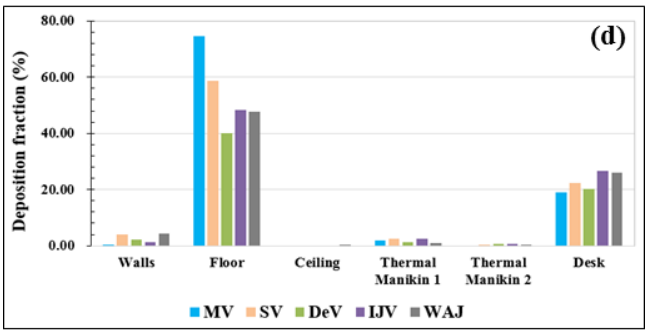
(d)
Deposition fraction (%)
80.00
60.00
40.00
20.00
0.00
Walls
Floor
Ceiling
Thermal Manikin 1
Thermal Manikin 2
Desk
MV
SV
DeV
IJV
WAJ

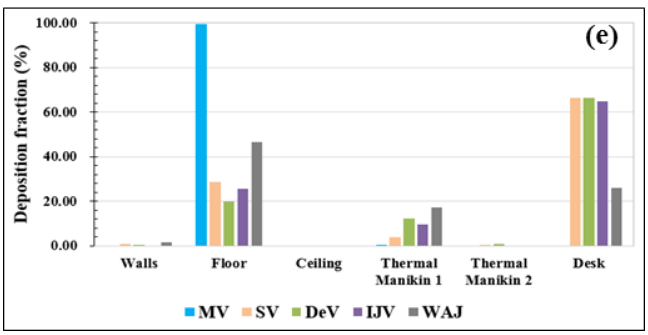
(e)
Deposition fraction (%)
100.00
80.00
60.00
40.00
20.00
0.00
Walls
Floor
Ceiling
Thermal Manikin 1
Thermal Manikin 2
Desk
MV
SV
DeV
IJV
WAJ

Fig. 11. Percentages of particles with five different diameters deposited on different surfaces. (a) 1 μm, (b) 5 μm, (c) 10 μm, (d) 30 μm, and (e) 50 μm.

3.2.4 Particle removal efficiency

Fig. 12 shows the information relating to the particle escape under five air distribution methods. The removal efficiency is defined as the ratio of the number of particles leaving the room via two exhaust outlets to the total number of particles released from the infector.

Removal of particles by the exhausts is widely regarded as an important way to improve indoor air quality, especially for fine particles (diameter ≤ 10 μm). As shown in Fig. 12, MV was significantly worse at removing fine particles than other four air distributions. The average removal efficiency of fine particles under MV was 27.61%, while the particle removal efficiencies of other four air distribution methods were all more than 35%. Furthermore, the removal efficiencies of fine particles under SV and DeV were increased by 24.82% and 35.41% respectively in comparison with MV. This demonstrates that DeV and SV are favorable in removing exhaled fine particles and reducing residual viral load in the air. The removal efficiencies of fine particles under IJV and WAJ were similar between 36% and 40%. For SV, DeV, IJV, and WAJ, the clean air could be transported to the occupied zone due to their effective airflow patterns. As a result, under the influence of positive thermal buoyancy, the upward flow of airflow can be helpful to carry exhaled fine particles to rise in heating mode. Nonetheless, the removal fraction decreases sharply when the particle diameter was larger than 30 μm. This showed that the particle removal efficiency has less dependence on the air distribution method as the particle size increased.

In addition, Fig. 12 shows the results of total particle removal efficiency. With the same supply air parameters (i.e., supply air temperature and airflow rate) and the same initial conditions of the particles, the results showed that DeV and SV had higher total particle removal efficiencies. Their removal efficiencies were 41.49% and 33.34% respectively, which were twice higher than that under

MV (i.e., 16.57%). For IJV and WAJ, the proportions of removed particles were 22.38%, and 27.54% respectively. Due to the larger range of recirculation zone formed in the room served by IJV, the particle removal efficiency under IJV is lower than that under WAJ. The total particle removal efficiency by the exhaust outlets ranged from approximately 16% to 42% under different air distribution methods. This implies that in heating mode, the air distribution method can have a significant influence on the removal of the exhaled particles.

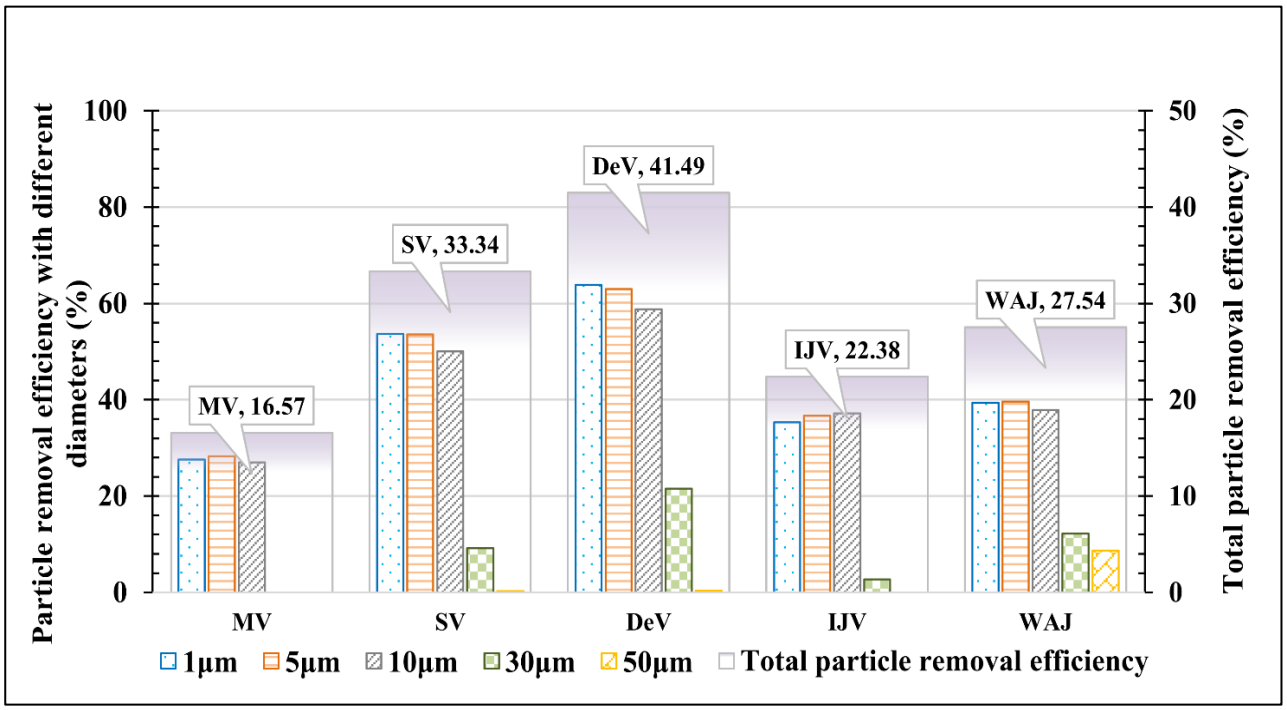

Fig. 12. Removal efficiency of particles with different diameters under five air distribution methods.

4. Discussion

The dispersion characteristics of exhaled particles under five typical air distribution methods with application potentials for heating were comprehensively investigated in this study. The results showed that the particle dispersion behaviors can be distinct under different air distribution methods. The difference of average normalized particle concentration at the breathing zone can be up to 8 times (4.45 under MV; 0.56 under SV) between MV and SV, and the maximum difference of total particle

removal efficiency was around 25% (41.49% under DeV; 16.57% under MV) between MV and DeV. For fine particles, there was a greater difference in the removal efficiency between the five air distribution methods, with a maximum difference of 35% (63.02% under DeV; 27.61% under MV). These results illustrated that the air distribution method was an important factor that affected the dispersion characteristics of exhaled particles for winter heating.

In the heating mode, all the air distribution methods investigated in this study can be affected by thermal buoyancy. The influence of thermal buoyancy on airflow largely depends on the layout and initial momentum of the supply air inlet. For MV, the thermal buoyancy resisted supply airflow from entering the occupied zone. Therefore, the negative effect of thermal buoyancy degraded inhaled air quality. However, for SV, DeV, IJV, and WAJ, the inlet layout and the momentum of supply air flow determined the volume of fresh air and the air velocity penetrating into the occupied zone. Then the airflow can carry particles under the influence of positive thermal buoyancy, which is beneficial to remove the exhaled particles. Meanwhile, the different directions of buoyancy force led to different air flow routes between winter and summer [33-34, 72-73], resulting in the difference in indoor particle dispersion, especially for fine particles. The results of this study showed that a large amount of fine particles was extracted through the exhausts under SV, DeV, IJV, and WAJ, which was consistent with the results of Zhou et al. [74] and Andrius et al.[75]. This was caused by the influence of positive thermal buoyancy on warm supply airflow in heating mode. Nevertheless, the rise of fine particles often only occurs around the heat source in summer [26, 34]. The investigation results of Tian et al. [19] and Wang et al. [26] showed that the fine particles were mainly removed by deposition on walls in summer. This indicated that the movement of particles was changed significantly with the air flow.

In this study, the particle concentration distributions under SV and DeV were similar, which was consistent with the results of Su et al. [34]. In their research, the supply airflow rate (i.e., 3.14 ACH)

was significantly lower than that of this study (i.e., 7.0 ACH). They emphasized that DeV might be better when the supply airflow rate was increased. However, the air velocity in the occupied zone under SV was higher, and more particles could be eliminated by deposition as compared with DeV. Meanwhile, the supply airflow of DeV collided with the deflector and then spread. The area affected by airflow in the occupied zone under DeV was wider than that under SV. Therefore, more particles were induced to the exhausts on the ceiling under DeV. There was little difference in particle concentration distribution and removal efficiency of fine particles between IJV and WAJ. Notably, WAJ performed better in removing coarse particles (diameter ≥ 30 μm). Presumably, it was because of the larger and stronger recirculation zone formed in the room served by IJV. In this circumstance, the recirculation zone formed by the airflow entrained the particles, and part of the particles could not reach the exhausts. Xing [76] found that the presence of obstacle on the air supply path caused a decline in the ventilation efficiency of IJV. Similarly, the results of this study showed that the ventilation efficiency might also be weakened by obstacles (e.g., the desk) in the vertical direction when IJV was used for heating in winter. For WAJ, the ventilation efficiency during heating can be improved by optimizing the supply air parameters. Yin et al. [73] showed that the range of the occupied zone covered by the warm airflow can be properly improved by changing the supply air velocity. In addition, the results of this study were consistent with some previous studies. Ren et al. [77] concluded that the risk of cross infection under SV was lower than that under MV. Furthermore, Ye et al. [78] found that the particle concentration at the breathing zone under MV was almost 3 times that under IJV, and IJV had the higher particle removal efficiency as compared with MV. For WAJ, adding a deflector can effectively reduce the pollutant concentration at the breathing zone, which has been demonstrated by Li et al. [33].

An appropriate air distribution method is crucial in controlling the spread of exhaled particles to the human body. Although MV had the highest indoor particle deposition fraction, it cannot be

considered as an efficient air distribution method in terms of the concentration distribution at the breathing zone and the particle removal efficiency. A higher removal efficiency indicates the less particles remaining in the room. Thus, the particle removal efficiency was used to indicate the efficiency of air distribution method in this study [16]. For the five air distribution methods, DeV had the best performance, followed by SV, WAJ, and then IJV. The removal efficiency for fine particles of DeV, SV, WAJ, and IJV were 61.86%, 52.43%, 38.95%, and 36.40% respectively. More than 35% of exhaled fine particles can be removed by using these air distribution methods. For DeV, the average removal efficiency of fine particles exceeded 60%. However, MV exhibited the worst performance. The removal efficiency of fine particles was the lowest, only 27.61%. The results of this study showed that air distribution methods, which can deliver clean air efficiently to the occupied zone, showed advantages in reducing the risk of virus transmission in winter.

Because of the complexity and uncertainty of the actual situation, one of the limitations for this study was that only some representative cases were simulated to compare the particle dispersion characteristics under five air distributions with typical layouts of inlets and outlets. Besides, this study was only conducted for the layout of a typical office. Due to the effect of intensified thermal plumes, the findings derived from this study may be unsuitable for multi-occupant spaces (e.g., classroom, conference room). Finally, this study simplified the complex periodic breathing activities into a constant exhalation. The impacts of such simplification remain to be further explored in future.

5. Conclusions

This study comprehensively investigated the dispersion characteristics of the exhaled particles from an infector under five air distributions methods (i.e., MV, SV, DeV, IJV, and WAJ) in a typical office room for winter heating. The airflow field, particle concentration distribution, particle residence time, deposition characteristics, and removal efficiency were compared. The main findings can be drawn as follows.

(1) The difference of average normalized particle concentration at the breathing zone under different air distribution methods can be up to 8 times, and the maximum difference of total particle removal efficiency can be more than 25%. These showed that air distribution methods can have significant impacts on the dispersion characteristics of exhaled particles in heating mode.

(2) Due to the influence of positive thermal buoyancy, the particle dispersion under different air distribution methods can be distinct from that in summer, especially for fine particles. For MV, the fresh air was difficult to enter the occupied zone in heating mode and did not dilute the particle concentration effectively. For SV, DeV, IJV, and WAJ, more fine particles can be carried to the upper zone of the room. The positive thermal buoyancy of indoor airflow made the main clearance mechanism of fine particles transformed from deposition in summer to removal in winter.

(3) By comparing the removal efficiency of exhaled particles, the ventilation performance of five air distribution methods in heating mode was evaluated. DeV had the best performance, followed by SV, WAJ, and then IJV. The average removal efficiency of fine particles under DeV exceeded 60%, which was twice higher than that under MV. The removal efficiency for fine particles of SV, WAJ, and IJV were 52.43%, 38.95%, and 36.40% respectively. For MV, the removal efficiency of particles for all sizes was the lowest, and the average removal efficiency of fine particles was only 27.61%.

Acknowledgments

This study is supported by National Natural Science Foundation of China (Grant No. 51978096). The authors expressed our thanks to Mr. Yunhao Li for his help in the experiments.

Reference

[1] JSM Peiris, KY Yuen, ADME Osterhaus, et al., The severe acute respiratory syndrome (SARS), The New England Journal of Medicine 349 (2003) 31-41.

https://doi.org/10.1056/NEJMra032498.

[2] IM Mackay, KE Arden, MERS coronavirus: diagnostics, epidemiology and transmission, Virology Journal 222 (2015). https://doi.org/10.1186/s12985-015-0439-5.

[3] SF Pedersen, YC Ho, SARS-CoV-2: a storm is raging, The Journal of clinical investigation, 130 (2020) 2202-2205. https://doi.org/10.1172/JCI137647.

[4] CDC (Centers for Disease Control and Prevention). https://www.cdc.gov/coronavirus/2019-ncov/prevent-getting-sick/how-covid-spreads.html.

[5] C Sun, Z Zhai, The efficacy of social distance and ventilation effectiveness in preventing COVID-19 transmission, Sustainable cities and society 62 (2020) 102390. https://doi.org/10.1016/j.scs.2020.102390.

[6] H Motamedi, M Shirzadi, Y Tominaga, et al., CFD modeling of airborne pathogen transmission of COVID-19 in confined spaces under different ventilation strategies, Sustainable Cities and Society 76 (2022) 103397. https://doi.org/10.1016/j.scs.2021.103397.

[7] Y Li, H Qian, J Hang, et al., Probable airborne transmission of SARS-CoV-2 in a poorly ventilated restaurant, Building and Environment 196 (2021) 107788. https://doi.org/10.1016/j.buildenv.2021.107788.

[8] HC. Burridge, RK. Bhagat, MEJ Stettler, et al., The ventilation of buildings and other mitigating measures for COVID-19: a focus on wintertime, The Royal Society 447 (2021). https://doi.org/10.1098/rspa.2020.0855.

[9] S Liu, M Koupriyanov, D Paskaruk, et al., Investigation of airborne particle exposure in an office with mixing and displacement ventilation, Sustainable Cities and Society 79 (2022) 103718. https://doi.org/10.1016/j.scs.2022.103718.

[10] S Zhang, D Niu, Z Lin, Occupancy-aided ventilation for airborne infection risk control: Continuously or intermittently reduced occupancies? Building Simulation (2022). https://doi.org/10.1007/s12273-022-0951-7.

[11] C Ren, H Chen, J Wang, et al., Ventilation impacts on infection risk mitigation, improvement of environmental quality and energy efficiency for subway carriages, Building and Environment 222 (2022) 109358. https://doi.org/10.1016/j.buildenv.2022.109358.

[12] JC Luongo, KP Fennelly, JA Keen, et al., Role of mechanical ventilation in the airborne transmission of infectious agents in buildings, Indoor air 26 (2016). https://doi.org/10.1111/ina.12267.

[13] S Srivastava, X Zhao, A Manay, et al., Effective ventilation and air disinfection system for reducing coronavirus disease 2019 (COVID-19) infection risk in office buildings, Sustainable Cities and Society 75 (2021) 103408. https://doi.org/10.1016/j.scs.2021.103408.

[14] X Tian, BZ Li, YX Ma, et al., Experimental study of local thermal comfort and ventilation performance for mixing, displacement and stratum ventilation in an office, Sustainable Cities and Society 50 (2019) 101630. https://doi.org/10.1016/j.scs.2019.101630.

[15] XF Kong, YF Chang, NN Li, et al., Comparison study of thermal comfort and energy saving under eight different ventilation modes for space heating, Build Simul 15 (2022) 1323–1337. https://doi.org/10.1007/s12273-021-0814-7.

[16] B Zhao, Y Zhang, X Li, et al., Comparison of indoor aerosol particle concentration and deposition in different ventilated rooms by numerical method, Building and Environment 39 (2004) 1-8. https://doi.org/10.1016/j.buildenv.2003.08.002.

[17] Z Lin, TT Chow, CF Tsang, Stratum ventilation? A conceptual introduction, Proceeding of the 10th International Conference on Indoor Air Quality and Climate, 2005.

[18] Z Lin, J Wang, T Yao, TT Chow, Investigation into anti-airborne infection performance of stratum ventilation, Building and Environment 54 (2012) 29-38. https://doi.org/10.1016/j.buildenv.2012.01.017.

[19] L Tian, Z Lin, Q Wang, J Liu, Numerical investigation of indoor aerosol particle dispersion under stratum ventilation and under displacement ventilation, Indoor and Built Environment 18 (2009) 360-375. https://doi.org/10.1177/1420326X09337335.

[20] YL Lu, Z Lin, Coughed droplet dispersion pattern in hospital ward under stratum ventilation, Building and Environment 208 (2022) 108602. https://doi.org/10.1016/j.buildenv.2021.108602.

[21] YL Lu, M Oladokun, Z Lin, Reducing the exposure risk in hospital wards by applying stratum ventilation system, Building and Environment 183 (2020) 107204. https://doi.org/10.1016/j.buildenv.2020.107204.

[22] XF Kong, CL Guo, Z Lin, S Duan, et al., Experimental study on the control effect of different ventilation systems on fine particles in a simulated hospital ward, Sustainable Cities and Society 73 (2021) 103102. https://doi.org/10.1016/j.scs.2021.103102.

[23] T Karimipanah, HB Awbi, Theoretical and experimental investigation of impinging jet ventilation and comparison with wall displacement ventilation, Building and Environment 37 (2002) 1329-1342. https://doi.org/10.1016/S0360-1323(01)00117-2.

[24] B Yang, AK Melikov, A Kabanshi, et al., A review of advanced air distribution methods-theory, practice, limitations and solutions, Energy and Buildings 202 (2019) 109359. https://doi.org/10.1016/j.enbuild.2019.109359.

[25] A Staveckis, A Borodinecs, Impact of impinging jet ventilation on thermal comfort and indoor air quality in office buildings, Energy & Buildings 235 (2021) 110738.

https://doi.org/10.1016/j.enbuild.2021.110738.

[26] L Wang, X Dai, J Wei, et al., Numerical comparison of the efficiency of mixing ventilation and impinging jet ventilation for exhaled particle removal in a model intensive care unit, Building and Environment 200 (2021). https://doi.org/10.1016/j.buildenv.2021.107955.

[27] Z Zhang, L Zeng, H Shi, et al., CFD Study on the Ventilation Effectiveness in a Public Toilet under Three Ventilation Methods, Energies 14 (2021) 8379. https://doi.org/10.3390/en14248379.

[28] X Ye, YM Kang, F Yang, et al., Comparison study of contaminant distribution and indoor air quality in large-height spaces between impinging jet and mixing ventilation systems in heating mode, Building and Environment 160 (2019) 106159. https://doi.org/10.1016/j.buildenv.2019.106159.

[29] AG Li, Extended Coanda Effect and attachment ventilation, Indoor and Built Environment 28 (2019) 437-442. https://doi.org/10.1177/1420326X19833850.

[30] H Yin, Study on air distribution characteristics and design method of vertical wall attached jet mode formed by slot air supply intlet, Xi'an University of architecture and technology, China, 2013.

[31] HG Yin, DN Ji, YY Wang, et al., Numerical study of particle spatial distribution under column attachment ventilation, Journal of Building Engineering 53 (2022) 104599. https://doi.org/10.1016/j.jobe.2022.104599.

[32] Z Lin, TT Chow, Y Li, Deflection ventilation - a conceptual introduction, Proceedings of 7th International Conference Healthy Buildings 2003. Stallion Press, Singapore, pp. 363-369.

[33] AG Li, Y Zhang, O Han, et al., Effectiveness of air distribution and pollutant control in

isolation wards, Heat. Vent. Air Cond 50 (2020) 26-34.

[34] W Su, B Yang, A Melikov, et al., Infection probability under different air distribution patterns, Building and Environment 207 (2022). https://doi.org/10.1016/j.buildenv.2021.108555.

[35] MNA Saïd, RA MacDonald, GC Durrant, Measurement of thermal stratification in large single-cell buildings, Energy and buildings 24 (1996): 105-115. https://doi.org/10.1016/0378-7788(95)00966-3.

[36] F Cheng, S Zhang, S Gao, et al., Experimental investigation of airflow pattern and turbulence characteristics of stratum ventilation in heating mode, Building and Environment 186 (2020) 107339. https://doi.org/10.1016/j.buildenv.2020.107339.

[37] The statistics data on COVID-19 of WHO (World Health Organization), March 2022. https://covid19.who.int/.

[38] TJ Meerhoff, JW Paget, JL Kimpen, et al., Variation of respiratory syncytial virus and the relation with meteorological factors in different winter seasons, The Pediatric infectious disease journal 28 (2009) 860-866. https://doi.org/10.1097/INF.0b013e3181a3e949.

[39] AD Storms, MD Van Kerkhove, E Azziz-Baumgartner, et al., Worldwide transmission and seasonal variation of pandemic influenza A (H1N1) 2009 virus activity during the 2009-2010 pandemic, Influenza and other respiratory viruses 6 (2013) 1328-1335. https://doi.org/10.1111/irv.12106.

[40] JW Tang, The effect of environmental parameters on the survival of airborne infectious agents, Journal of the Royal Society Interface 6 (2009) 737-746. https://doi.org/10.1098/rsif.2009.0227.focus.

[41] HT Dao, KS Kim, Behavior of cough droplets emitted from COVID-19 patient in hospital

isolation room with different ventilation configurations, Building and Environment 209 (2022) 108649. https://doi.org/10.1016/j.buildenv.2021.108649.

[42] J Wang, Numerical study on evaporation and dispersion process of personnel exhaled droplets, Southeast University, China, 2011.

[43] M Jayaweera, H Perera, B Gunawardana, et al., Transmission of COVID-19 virus by droplets and aerosols: A critical review on the unresolved dichotomy, Environmental research 188 (2020) 109819. https://doi.org/10.1016/j.envres.2020.109819.

[44] Q Zhou, H Qian, H Ren, et al., The lock-up phenomenon of exhaled flow in a stable thermally-stratified indoor environment, Building and Environment 116 (2017) 246-256. https://doi.org/10.1016/j.buildenv.2017.02.010.

[45] C Ren, C Xi, J Wang, Z Feng, et al., Mitigating COVID-19 infection disease transmission in indoor environment using physical barriers, Sustainable Cities and Society 74 (2021) 103175. https://doi.org/10.1016/j.scs.2021.103175.

[46] Y Cheng, Z Lin, Experimental investigation into the interaction between the human body and room airflow and its effect on thermal comfort under stratum ventilation, Indoor air 26 (2016) 274-285. https://doi.org/10.1111/ina.12208.

[47] S Zhang, Z Lin, Z Ai, et al., Multi-criteria performance optimization for operation of stratum ventilation under heating mode, Applied energy 239 (2019) 969-980. https://doi.org/10.1016/j.apenergy.2019.01.248.

[48] Y Li, Study on airflow distribution characteristics and thermal comfort of deflection ventilation for heating, Chongqing University, China, 2021.

[49] JA Khan, CE Feigley, E Lee, et al., Effects of inlet and exhaust locations and emitted gas

density on indoor air contaminant concentrations, Building and Environment 41 (2006) 851–863. https://doi.org/10.1016/j.buildenv.2005.04.002.

[50] Z Zhai, Z Zhang, W Zhang, et al., Evaluation of various turbulence models in predicting airflow and turbulence in enclosed environments by CFD: Part 1-Summary of prevalent turbulence models, HVAC and R Research 13 (2007) 853-870.

[51] PV Nielsen, Computational fluid dynamics and room air movement, Indoor air 14 (2004) 134-143. https://doi.org/10.1111/j.1600-0668.2004.00282.x.

[52] F Chen, H Chen, J Xie, et al., Air distribution in room ventilated by fabric air dispersion system, Building and Environment 46 (2011) 2121-2129. https://doi.org/10.1016/j.buildenv.2011.04.016.

[53] INC. A. ANSYS Fluent User's Guide 19 R1, 2019.

[54] L Tian, Z Lin, Q Wang, Comparison of gaseous contaminant diffusion under stratum ventilation and under displacement ventilation, Building and Environment 45 (2010) 2035-2046. https://doi.org/10.1016/j.buildenv.2010.01.002.

[55] N Gao, J Niu, Modeling particle dispersion and deposition in indoor environments, Atmospheric environment 41 (2007) 3862-3876. https://doi.org/10.1016/j.atmosenv.2007.01.016.

[56] H Qian, Y Li, Removal of exhaled particles by ventilation and deposition in a multibed airborne infection isolation room, Indoor air 20 (2010) 284-297. https://doi.org/10.1111/j.1600-0668.2010.00653.x.

[57] C Chen, B Zhao, W Cui, et al., The effectiveness of an air cleaner in controlling droplet/aerosol particle dispersion emitted from a patient's mouth in the indoor environment

of dental clinics, Journal of the Royal Society Interface 7 (2010) 1105-1118. https://doi.org/10.1098/rsif.2009.0516.

[58] Y Wang, S Wu, Y Yang, et al., Evaporation and movement of fine droplets in non-uniform temperature and humidity field, Building and Environment 150 (2019) 75-87. https://doi.org/10.1016/j.buildenv.2019.01.003.

[59] GB 50736-2012, Design code for heating, ventilation and air conditioning of civil buildings, Ministry of Housing and Urban-Rural Development of the People's Republic of China, Beijing, China, 2012.

[60] GB50189-2015, Design standard for energy efficiency of public buildings, China Construction Industry Press, China, 2015.

[61] R Cermak, AK Melikov, Protection of occupants from exhaled infectious agents and floor material emissions in rooms with personalized and underfloor ventilation, HVAC and R Research 13 (2007) 23-38.

[62] Q He, J Niu, N Gao, et al., CFD study of exhaled droplet transmission between occupants under different ventilation strategies in a typical office room, Building and Environment 46 (2011) 397-408. https://doi.org/10.1016/j.buildenv.2010.08.003.

[63] N Mao, CK An, L Guo, et al., Transmission risk of infectious droplets in physical spreading process at different times: a review, Building and Environment 185 (2020) 107307. https://doi.org/10.1016/j.buildenv.2020.107307.

[64] J Pantelic, KW Tham, D Licina. Effectiveness of a personalized ventilation system in reducing personal exposure against directly released simulated cough droplets. Indoor Air 25 (2015) 683-693. https://doi.org/10.1111/ina.12187.

[65] C Chen, B Zhao, Some questions on dispersion of human exhaled droplets in ventilation room: answers from numerical investigation, Indoor Air 20 (2010) 95–111. https://doi.org/10.1111/j.1600-0668.2009.00626.x.

[66] Y Cheng, Experimental and numerical study of air distribution characteristics and thermal environment under stratum ventilation, City University of Hong Kong, China, 2015.

[67] A ElHaroun, EE Khalil, A Fahim, et al., Analyses of thermal comfort and indoor air quality under stratum, displacement and mixing ventilation systems, AIAA Propulsion and Energy Forum: 13th International Energy Conversion Engineering Conference, 2015.

[68] Q Chen, Numerical and experimental study of downward directed vertical wall jets induced ventilation system in ship cabins, Huazhong University of Science & Technology, China, 2015.

[69] F Chen, CM Simon, ACK Lai, Modeling particle distribution and deposition in indoor environments with a new drift–flux model, Atmospheric Environment 40 (2006) 357-367. https://doi.org/10.1016/j.atmosenv.2005.09.044.

[70] ANSI/ASHRAE Standard 55-2020, Thermal Environmental Conditions for Human Occupancy, American Society of Heating, Refrigerating and Air-Conditioning Engineers, Atlanta, GA, USA, 2020.

[71] S Zhang, YL Lu, D Niu, et al., Energy performance index of air distribution: Thermal utilization effectiveness, Applied Energy 307 (2022) 118122. https://doi.org/10.1016/j.apenergy.2021.118122.

[72] Z Lin, Stratum ventilation - a low-carbon way to thermal comfort and indoor air quality, International Journal of Low-Carbon Technologies 12 (2017) 323-329. https://doi.org/10.1093/ijlct/ctw020.

[73] HG Yin, YK Huo, YY Wang, et al., Numerical investigation on mechanisms and performance of column attachment ventilation for winter heating, Building and Environment 202 (2021) 108025. https://doi.org/10.1016/j.buildenv.2021.108025.

[74] Y Zhou, YL Deng, P Wu, et al., The effects of ventilation and floor heating systems on the dispersion and deposition of fine particles in an enclosed environment, Building and Environment 125 (2017) 192-205. https://doi.org/10.1016/j.buildenv.2017.08.049.

[75] A Jurelionis, L Gagyte, L Seduikyte, et al., Combined air heating and ventilation increases risk of personal exposure to airborne pollutants released at the floor level, Energy and Buildings 116 (2016) 263-273. https://doi.org/10.1016/j.enbuild.2016.01.011.

[76] Y Xing, Numerical simulation of indoor air quality in the condition of impinging jet vetilation, Chongqing University, China, 2012.

[77] C Ren, HC Zhu, SJ Cao, Ventilation strategies for mitigation of infection disease transmission in an indoor environment: a case study in office, Buildings 12 (2022). https://doi.org/10.3390/buildings12020180.

[78] X Ye, YM Kang, F Yang, et al., Comparison study of contaminant distribution and indoor air quality in large-height spaces between impinging jet and mixing ventilation systems in heating mode, Building and Environment 160 (2019) 106159. https://doi.org/10.1016/j.buildenv.2019.106159.